Sensors & Actuators: B. Chemical 304 (2020) 127267

Contents lists available at ScienceDirect

Sensors and Actuators B: Chemical

journal homepage: www.elsevier.com/locate/snb

Dual-mode amplified detection of rabies virus oligonucleotide via Y-shaped DNA assembly

Jiaojiao Zhou[a,1], Wenjing Wang[a,1], Shuojun Li[a], Axiu Nie[a], Zhiyong Song[a], Mohamed F. Foda[a,b], Zhicheng Lu[a], Ling Zhao[a], Heyou Han[a,*]

[a] State Key Laboratory of Agricultural Microbiology, College of Food Science and Technology, College of Science, College of Veterinary Medicine, Huazhong Agricultural University, Wuhan 430070, China
[b] Department of Biochemistry, Faculty of Agriculture, Benha University, Moshtohor, Toukh, 13736, Egypt

ARTICLE INFO

Keywords:
Y-shaped DNA
Fluorescence
Enzyme cascade
CHA
RABV oligonucleotide

ABSTRACT

An innovative fluorescent and colorimetric dual-mode strategy based on Y-shaped DNA was proposed for the detection of rabies virus oligonucleotide. The cascade assembly of hairpin probes was initiated by the target, leading to the formation of Y-shaped DNA accompanied by freeing target to catalyze the next assembly process. The fluorescence recovery of the fluorophore FAM was accompanied by opening of hairpin probe. A colorimetric signal was generated by the proximity of glucose oxidase (GOx) and horseradish peroxidase (HRP), which was reflected by enhanced catalytic capability to TMB. Using this method, target DNA can be detected with a wide linear range from 0.1 to 6 nM with a detection limit of 15 pM, and from 0.5 to 60 nM with a detection limit of 60 pM for fluorescent and colorimetric readout, respectively. Moreover, the dual-mode detection strategy exhibited excellent selectivity towards the target compared with interference oligonucleotides. In addition, recoveries ranging from 96.0% to 106% with RSD values varying from 3.2% to 5.4%, and from 91.0% to 102% with RSD values varying from 3.3% to 7.1% for fluorescent and colorimetric studies, respectively, were obtained in diluted cerebrospinal fluid samples. The proposed dual-mode sensor is easy to operate with excellent detection performance. It would be superior to single mode detection and more practicable for quantitative detection of nucleic acid-related biomarkers due to the self-correction capability.

1. Introduction

Nucleic acid detection at trace levels plays a significant role in identification and diagnosis of viral infections [1,2], cancer [3,4], and other diseases [5,6]. Given the low amount of specific target in a biological system, a variety of powerful signal amplification techniques have been established [7–10], which promote the detection sensitivity and dynamic range of nucleic acid-related biomarkers. Among them, entropy-driven catalysis based signal amplification strategies [11,12], in particular those operated at constant room temperature, including hybridization chain reaction (HCR) [13] and catalytic hairpin assembly (CHA) [14], pave the way for the detection of low-abundance nucleic acids. Such mechanisms have gained comprehensive attention recently in the field of biosensing research [15,16]. They were coupled with a series of detection techniques, including electrochemical, fluorescent, and colorimetric methods to achieve sensitive detection of trace amount nucleic acids, proteins, and small molecules with negligible background [17,18].

CHA is the most representative example developed and is catalyzed by targeted toehold-mediated strand displacement reactions. It has been adapted to a series of applications, including nucleic acid detection [19], biological molecule imaging [20], and cancer therapy [21]. Diverse DNA structure assemblies including G-quadruplexes [22] and Y-shaped DNA [23,24], can be either formed *in situ* or incorporated in the final products by CHA, providing unlimited possibilities for biosensing signal transduction. Among them, Y-shaped DNA has been widely applied due to its simple structure and high stability. However, its properties haven't been fully exploited for the following reasons: (1) only one-arm of the Y-shaped DNA is used to produce signal and the other two arms do not participate the process, limiting the signal amplification efficiency [25] and (2) most Y-shaped DNA based amplified biosensing platforms analyze targets based on a single signal readout [16,26], either colorimetric or fluorescent, which may be influenced by external interferences such as different operating personnel. Coupling

* Corresponding author.
E-mail address: hyhan@mail.hzau.edu.cn (H. Han).
[1] Equal contribution.

https://doi.org/10.1016/j.snb.2019.127267
Received 12 April 2019; Received in revised form 8 October 2019; Accepted 9 October 2019
Available online 17 October 2019
0925-4005/ © 2019 Elsevier B.V. All rights reserved.

dual-mode detection in a single Y-shaped DNA structure would be an ideal solution for these limitations. Therefore, it is imperative to construct a more effective Y-shaped DNA based biosensing system.

Alternatively, the enzyme cascade reaction has been recognized as another simple and efficient signal amplification method for biomolecular detection [27]. The advantages of DNA nanotechnology, especially the site-specific addressability, allow precise tuning of the distance between enzyme pairs, permitting successful control of the enzyme cascade activity [28–31]. Once enzymes are located onto the DNA nanostructures within appropriate distances, the catalytic activity would be obviously enhanced. As a result, qualitative evaluation of target DNA is achieved via visual observation due to the generation of colored product, providing a versatile strategy for amplified point of care (POC) biosensing [32].

In this manuscript, in order to make full use of Y-shaped DNA nanostructures, we incorporated cascade enzyme pairs into the detection system to carry out amplified dual-mode biosensing. To the best of our knowledge, this is the first report on the utilization of Y-shaped DNA for development of fluorescent and colorimetric dual-mode detection. As a proof-of-concept, rabies virus (RABV) oligonucleotide (short segment: 5′-TGGACTAATAACTGAAACTTATGT-3′, 24-bases, X03673.1) was chosen as the model analyte because rabies remains the only disease with a 100% mortality rate [33,34]. According to literature, this oligonucleotide is a conservative sequence that has been identified as a biomarker of rabies [35,36]. It is of urgent demand for a rapid and sensitive detection method for RABV. The detection principle is shown in Scheme 1. Three metastable hairpin DNA probes (HP-A, HP-B, and HP-C) were employed, and each probe was designed with a stem of 18 base pairs and an additional 6 nucleotide sticky end at the 5′-end. Initially, the HP-A, labeled with a fluorophore (FAM) at 5′-end and a quencher (BHQ1) at the 3′-end, formed a stem-loop hairpin structure through Watson-crick interaction between the complementary sequences. HP-B and HP-C were functionalized with glucose oxidase (GOx) and horseradish peroxidase (HRP) at the 3′ end, respectively. In the absence of the target, weak fluorescence signal was observed due to the intrinsic intramolecular fluorescence resonance energy transfer (FRET) for HP-A. These three probes can coexist stably together. The introduction of target activated the CHA of HP-A, GOx-B, and HRP-C, producing the Y-shaped DNA nanostructures consisting of three hairpin probes, along with the fluorescence recovery of HP-A and the catalytic cascades of GOx and HRP caused by the distance proximity. Upon the addition of 3, 3, 5, 5-Tetramethyl benzidine (TMB) and glucose, the glucose was oxidized by GOx, generating gluconic acid and hydrogen peroxide (H_2O_2). H_2O_2 acts as substrate for HRP, allowing the effective oxidation of TMB to the colored product of oxTMB ($\lambda = 652$ nm). As a result, the restored fluorescence and the subsequent colored product can be used for expedient dual-mode signal readout. Each assembly process was followed by a disassembly step in which HP-C displaced the target from the complex, releasing the target to trigger the next assembly process for signal amplification. In this regard, the amplified intensity of restored fluorescence and absorbance of oxTMB was related to the concentration of the target. The dual-mode detection strategy based on single Y-shaped DNA is superior to single mode due to the combination of qualitative and quantitative detection by elimination of external interferences. Moreover, the method can be applied in complex biological matrices such as serum. With the advantages of excellent sensitivity, simple operation, fast speed, and quantitative read-out, this sensor holds great potential for nucleic acid target detection.

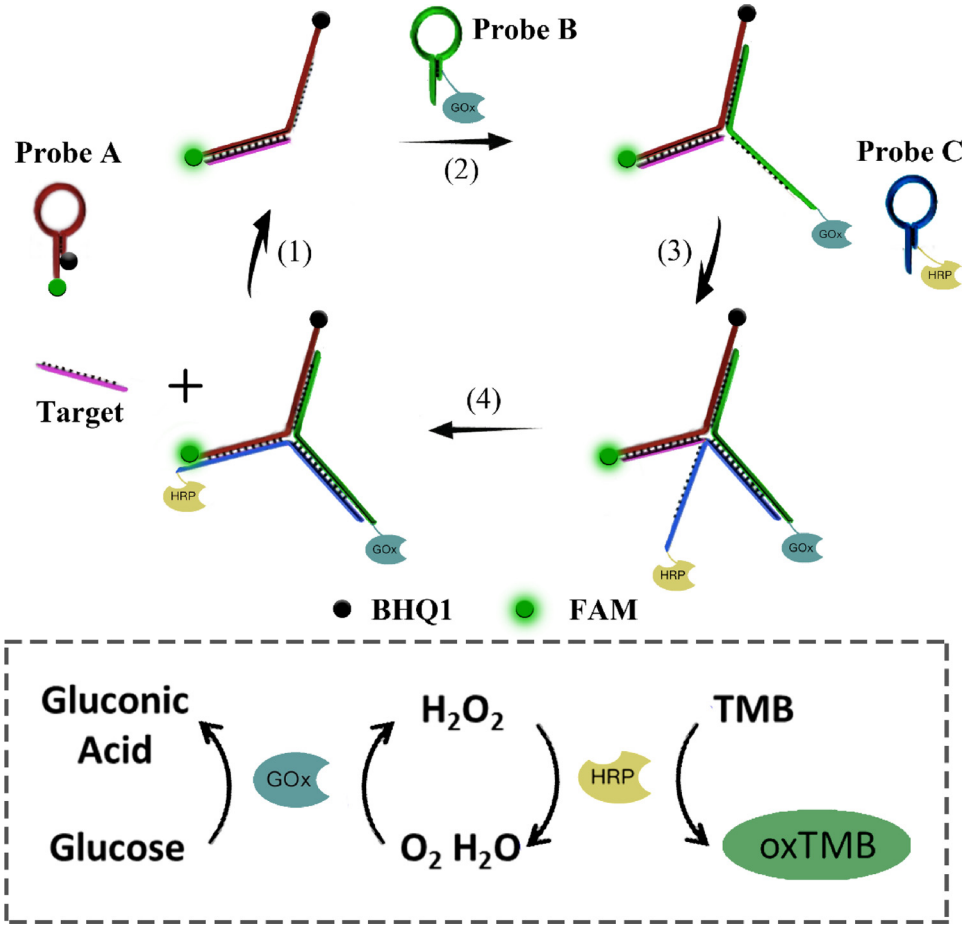

Scheme 1. Schematic illustration of the proposed Y-shaped DNA nanostructure-based dual-mode strategy for the amplified detection of rabies virus oligonucleotide. Note: The picture is not drawn in accordance with the actual proportion.

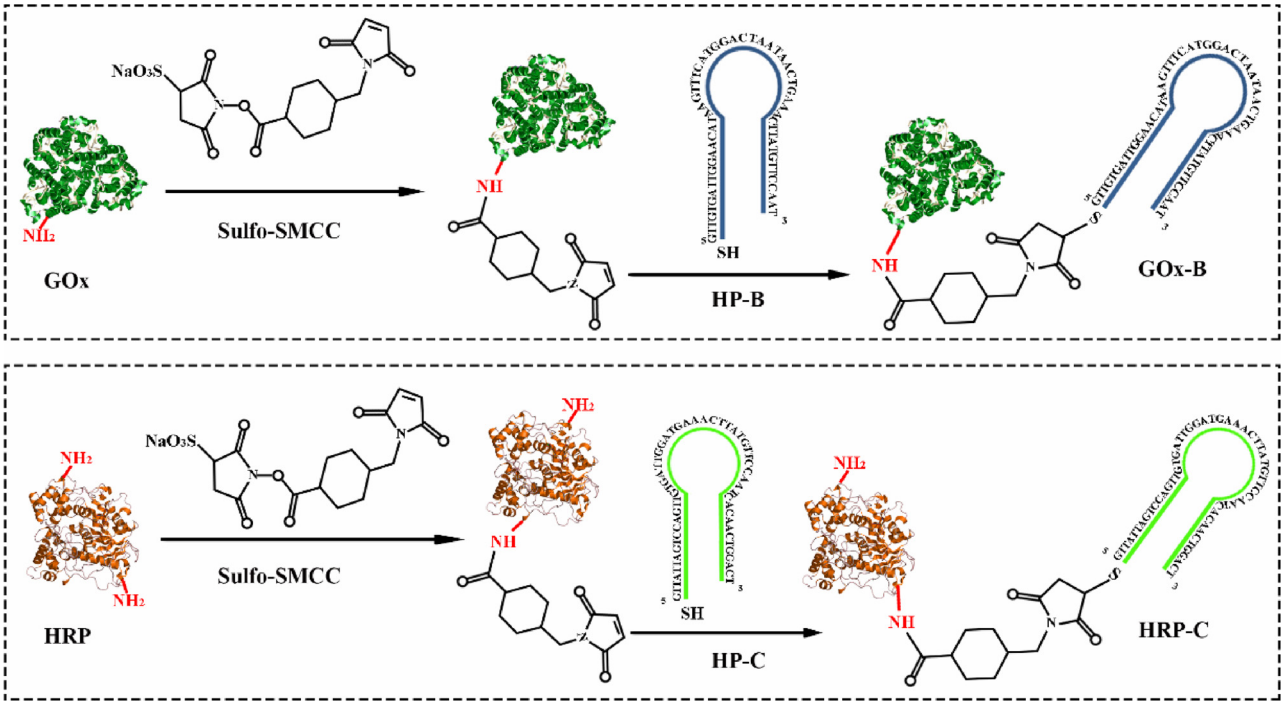

Fig. 1. Schematic illustration of the sulfo-SMCC conjugation chemistry used for enzyme-DNA conjugation. (note: GOx and HRP were drawn according to the Protein Data Bank (http://www.rcsb.org); The structure of sulfo-SMCC was drawn using ChemDraw).

2. Materials and methods

2.1. Chemicals and materials

Tris (2-carboxyethyl) phosphine hydrochloride (TCEP, ≥ 98%) was purchased from Sigma-Aldrich (St. Louis, MO, USA). Acrylamide mix solution (40% w/v), ammonium persulfate (APS, ≥ 99%), 1,2-bis(dimethylamino)-ethane (TEMED, ≥ 99.0%), sulfosuccinimidyl-4-(N-maleimidomethyl)cyclohexane-1-carboxylate (sulfo-SMCC, > 98%), and low range DNA ladder (25 ~ 500 bp) were obtained from Sangon Biotechnology Co. Ltd. (Shanghai, China). GOx and HRP were bought from Aladdin Chemical Co. Ltd. (Shanghai, China). Fetal bovine serum (FBS) was purchased from GIBCO Invitrogen Corp. All the oligonucleotides involved were synthesized and purified by Sangon Biotechnology Co. Ltd. (Shanghai, China); the detailed sequences are listed in Table S1. The secondary structures were provided by IDT Oligo Analyzer (https://sg.idtdna.com/pages) as shown in Fig. S1, the melting temperatures were all designed to be above 60 °C to increase the stability and decrease non-specific leakage reaction possibility. All the other reagents were analytically pure and used without any purification. Deionized (DI) water obtained from a Millipore water purification system (Milli-Q, Millipore, 18.2 MΩ resistivity) was used throughout this study.

2.2. Apparatus

Ultraviolet-visible (UV–vis) absorption spectroscopy was carried out on a UV-1800 spectrometer (Shimadzu, Japan). The concentration of oligonucleotide was determined on a DS-11 spectrophotometer (DeNovix, USA). The fluorescence intensity measurements were recorded by a RF-6000 spectrofluorophotometer (Shimadzu, Japan).

2.3. Enzyme conjugation with hairpin DNA probes

The GOx conjugated HP-B (GOx-B) and HRP conjugated HP-C (HRP-C) were prepared by using sulfo-SMCC as a heterobifunctional linker. Briefly, prior to modification, the thiol-DNA (30 μL of 100 μM) was activated by 3 μL of 100 M TCEP at pH 5.2 for 1 h at room temperature, the excess TCEP was separated by a cutoff filter (Amicon, 3 kDa). Then, 12 μL of 25 μM enzyme was mixed with a 20-fold excess sulfo-SMCC and incubated for 1 h at room temperature in 1 × PBS solution (with 100 mM NaCl, pH = 7.4), allowing the covalent conjugation of the N-hydroxysuccinimide (NHS) ester group of sulfo-SMCC with primary amines of the enzyme to form amide bonds. The excess sulfo-SMCC was separated using a cutoff filter (Amicon, 10 kDa). The purified solution of sulfo-SMCC modified enzyme was further coupled with 30 μL of 100 μM thiol-DNA for 48 h at 25 °C. In this respect, the maleimide group of the sulfo-SMCC molecule reacted with the sulfhydryl group at pH 7.4 to form stable thioether bonds. Finally, this mixture was purified by a cutoff filter (Amicon, 30 kDa) and stored at 4 °C for further use.

2.4. Procedure of dual-modal fluorescent and colorimetric measurements

In brief, a series of different concentrations of target were mixed with the solution of 10^{-4} M of HP-A, GOx-B, and HRP-C, to a final volume of 0.1 mL. The fluorescence measurements were recorded under the excitation wavelength at 490 nm. Subsequently, glucose and TMB were added to the formed Y-shaped enzyme cascade system for the collection of colorimetric signals. The absorbance intensities were monitored via a SpectraMax i3x at an absorption wavelength of 652 nm.

2.5. Detection of RABV oligonucleotide in complex matrices

To test the feasibility of our proposed strategy for detecting the target in complex matrices, FBS was mixed with the target for preparation of spiked samples. Then, the detection procedure was carried out following the procedure described, and the recovery was finally calculated. Control experiments were the same except that no target was added. To further assess the utility of the proposed biosensor, the recovery experiments were performed by spiking different concentrations of target into normal cerebrospinal fluid samples obtained from Huazhong Agricultural University (Wuhan, China).

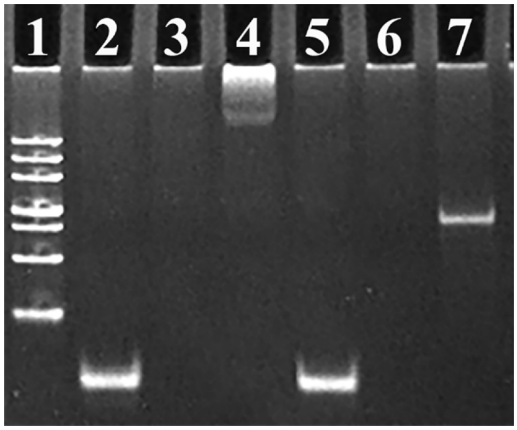

Fig. 2. 8% native PAGE characterization of the enzyme modified hairpin probes. (1) 500 bp DNA marker; (2) HP-B; (3) GOx; (4) GOx-B; (5) HP-C; (6) HRP; and (7) HRP-C.

3. Results and discussion

3.1. Preparation and characterization of enzyme-conjugated hairpin probes

The preparation of enzyme-conjugated hairpin probes was performed according to the previous literatures [27,37]. Sulfo-SMCC, a typical heterobifunctional protein crosslinker, was utilized to prepare enzyme-DNA conjugates. HP-B and HP-C were synthesized with thiol group modification at the 3′-end. Then, a typical enzyme cascade pair (GOx/HRP) was employed to conjugate with HP-B and HP-C by sulfo-SMCC to prepare the enzyme functionalized hairpin probes (GOx-B/HRP-C) (Fig. 1).

To characterize whether enzyme-DNA complexes (GOx-B/HRP-C) had been successfully formed, an 8% native PAGE was firstly performed. The native PAGE procedures are presented in the Supporting Information. DNA strands can be stained effectively by YeaRed Nucleic Acid Gel Stain solution in native PAGE. As shown in Fig. 2, bright bands were clearly observed for pure hairpin probes (HP-B/HP-C, lanes 2 & 5). Pure enzymes (GOx/HRP, lanes 3 & 6) could not be stained on the gel. After conjugation, enzyme-DNA complexes (GOx-B/HRP-C) presented new bright bands (lanes 4 & 7) due to their greater molecular weights than pure hairpin strands, indicating the successful formation of GOx-B/HRP-C probes. Notably, the GOx-B band migrated slower than that of HRP-C, indicating a larger molecular weight of GOx compared with HRP, which is consistent with previous findings [27,29]. UV-vis absorbance spectra were conducted subsequently to further confirm the as-prepared GOx-B/HRP-C probes (Fig. S2). The characteristic absorption peaks for the enzymes (450 nm for GOx, 403 nm for HRP) and DNA strands (260 nm) were observed for the GOx-B/HRP-C probes, which are consistent with a previous report [37], demonstrating the enzymes have been conjugated with DNA as expected for further use.

3.2. Feasibility study

To evaluate the feasibility of our design, a 2% agarose gel was employed to characterize the assembly of Y-shaped DNA, and the results are presented in Fig. 3**A**. The 500 bp DNA marker is shown in lane 1, and the three hairpin probes (HP-A, HP-B, and HP-C) are shown in lanes 2, 3, and 4, respectively. Minimal hairpin probe assembly took place in the absence of target (lane 6), and all probes assembled

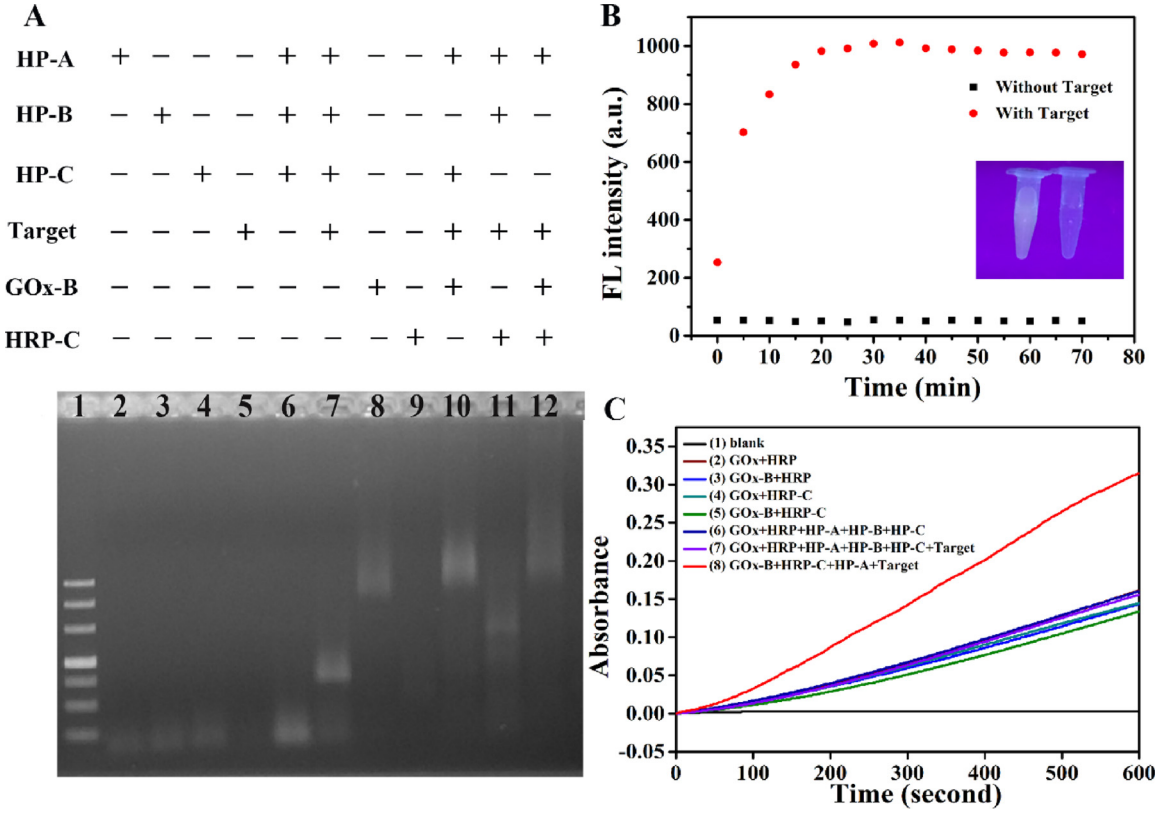

Fig. 3. Evidence for successful dual mode measurement. (A) Characterization of enzyme-functionalized Y-shaped DNA by agarose gel electrophoresis. (1) 500 bp DNA marker; (2) HP-A; (3) HP-B; (4) HP-C; (5) target; (6) HP-A + HP-B + HP-C; (7) HP-A + HP-B + HP-C + target; (8) GOx-B; (9) HRP-C; (10) GOx-functionalized Y-shaped DNA; (11) HRP-functionalized Y-shaped DNA; (12) enzyme pair- functionalized Y-shaped DNA. (B) Incubation time optimization by monitoring the real-time changes of FAM fluorescence. Inset shows fluorescent images under UV irradiation (left: with target, right: without target). (C) Real-time monitoring of absorbance in the presence of different complexes. The spectra were taken at 652 nm for oxTMB.

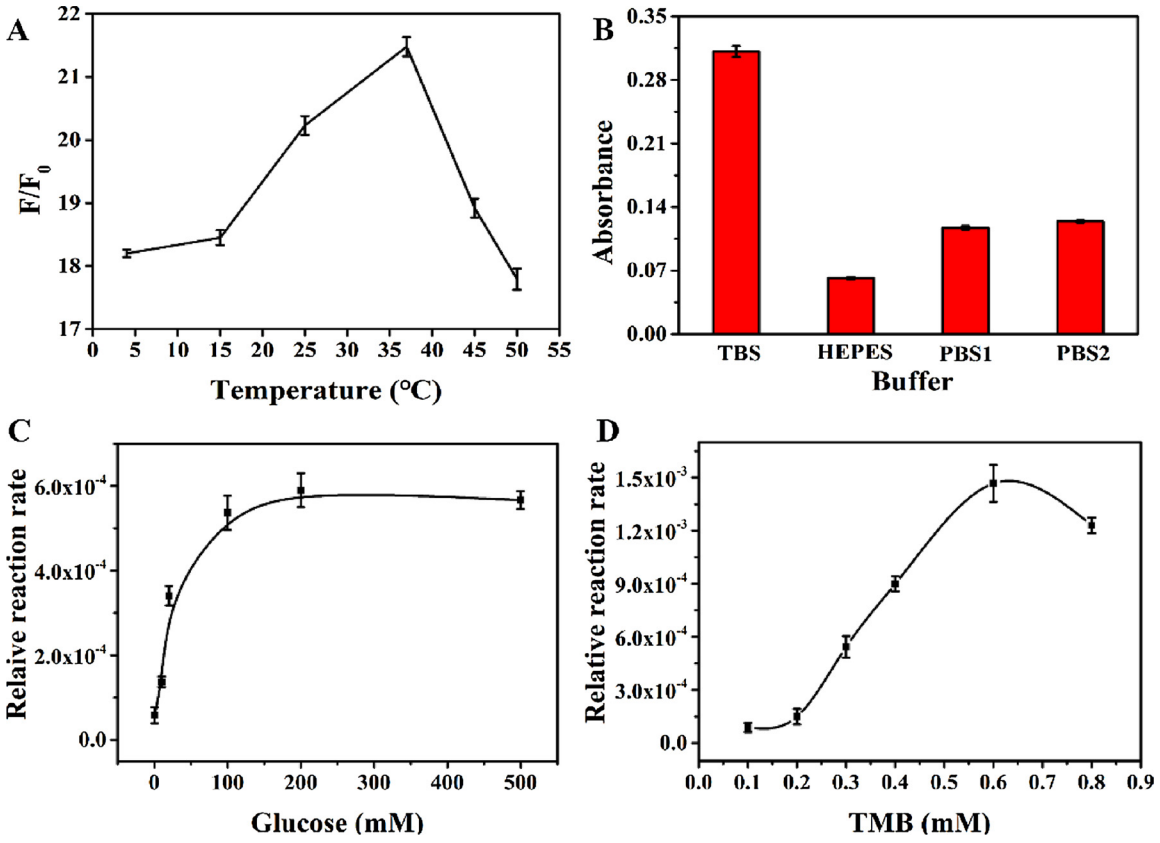

Fig. 4. Parameters optimization for dual mode measurement. (A) Effect of temperature on the fluorescent signal-to-background ratio (SBR) (SBR = F/F_0, where F, F_0 are the fluorescence intensity of FAM in the presence or absence of target DNA, respectively). (B) Optimization of constituents of buffer for colorimetric assay. (C, D) Optimization of concentrations of glucose and TMB for colorimetric assay, respectively.

obviously upon the addition of target (lane 7). This indicated that Y-shaped DNA was formed by target-catalyzed hybridization assembly. We incubated GOx-B and HRP-C with the other two pure hairpin DNA probes (lanes 10 and 11), leading to the formation of new band that migrated slower than the pure Y-shaped DNA shown on the gel (lane 7), suggesting that the conjugation of enzymes with hairpin probes did not affect the formation of Y-shaped DNA. Additionally, compared with GOx-B (lane 8), GOx-B formed Y-shaped DNA exhibited slower migration through the gel (lane 10), which further demonstrated successful nanostructure assembly. The band of lane 10 migrated slower than that of lane 11 because of the molecular weight difference between GOx and HRP. When both of the enzyme modified hairpin probes were incubated with HP-A (lane 12), there were no hairpin probes left in the system. This band displayed slower migration than those of single enzyme-modified DNA structures (lanes 10 and 11), suggesting that both enzymes were conjugated to the Y-shaped DNA. Conclusively, the rationally designed hairpin probes can successfully form Y-shaped DNA with addition of target, and the conjugation of enzymes with hairpin probes did not affect the formation of Y-shaped DNA.

With the enzyme conjugated hairpin probes at hand, the feasibility of dual-mode measurement was evaluated by monitoring the changes of fluorescent and colorimetric signals. Firstly, real-time monitoring of the fluorescent signal was conducted (Fig. 3B). Increasing fluorescence intensity was observed along with increasing reaction time after the addition of 3 nM target, and then plateaued after 20 min (red circle in Fig. 3B). In addition, a visible green color was observed in the presence of 1 μM target under UV light, while little background signal was observed in the absence of target (inset in Fig. 3B). These results suggested that Y-shaped DNA was formed accompanied by the recovery of fluorescence for HP-A. Thus, the target can be detected through the change of fluorescent signal. Then, the enzyme cascade catalytic capability of Y-shaped DNA was evaluated by the production rate of oxTMB. Both glucose and TMB were mixed with different systems by observing the increment of absorbance of oxTMB at 652 nm. As shown in Fig. 3C, the blank buffer showed no catalytic performance (line 1) and the system of free enzymes showed enhanced catalytic performance (line 2). The catalytic performance of the systems that contained one or both of the enzyme-conjugated hairpin DNA probes showed negligible changes (lines 3, 4, & 5) compared to the free enzymes systems (line 2). Furthermore, the simple mixture of free enzymes and hairpin DNA probes exhibited similar catalytic performance with free enzymes whether target existed or not (lines 2, 6, & 7). This is because the average distance between the free enzymes was the same when they were free in solution. It should be noted that the enzymes were dispersed in the solution irregularly on a micrometer-scale distance [29], with low catalytic capability. However, compared with free enzymes, the system consisting of both enzyme-conjugated hairpin DNA probes demonstrated a significantly enhanced catalytic performance in the presence of target (line 8). Enzyme pairs assembled on the Y-shaped DNA nanostructure afforded a much closer diffusion channel for H_2O_2. H_2O_2 was a key factor that influenced the catalytic rate according to previous work [38]. Therefore, when enzyme pairs were distributed on the Y-shaped DNA triggered by target, the distance between the enzyme pairs was reduced to nanometer-scale. The diffusion rate of H_2O_2 would be faster than that catalyzed by free enzymes, which can be explained by three-dimensional diffusion model according to Yan's research [38]. The H_2O_2 generated by GOx formed a high local concentration adjacent to HRP and accelerated the oxidation of TMB accordingly [29,37]. Finally, this enhancement of absorbance was used for target detection.

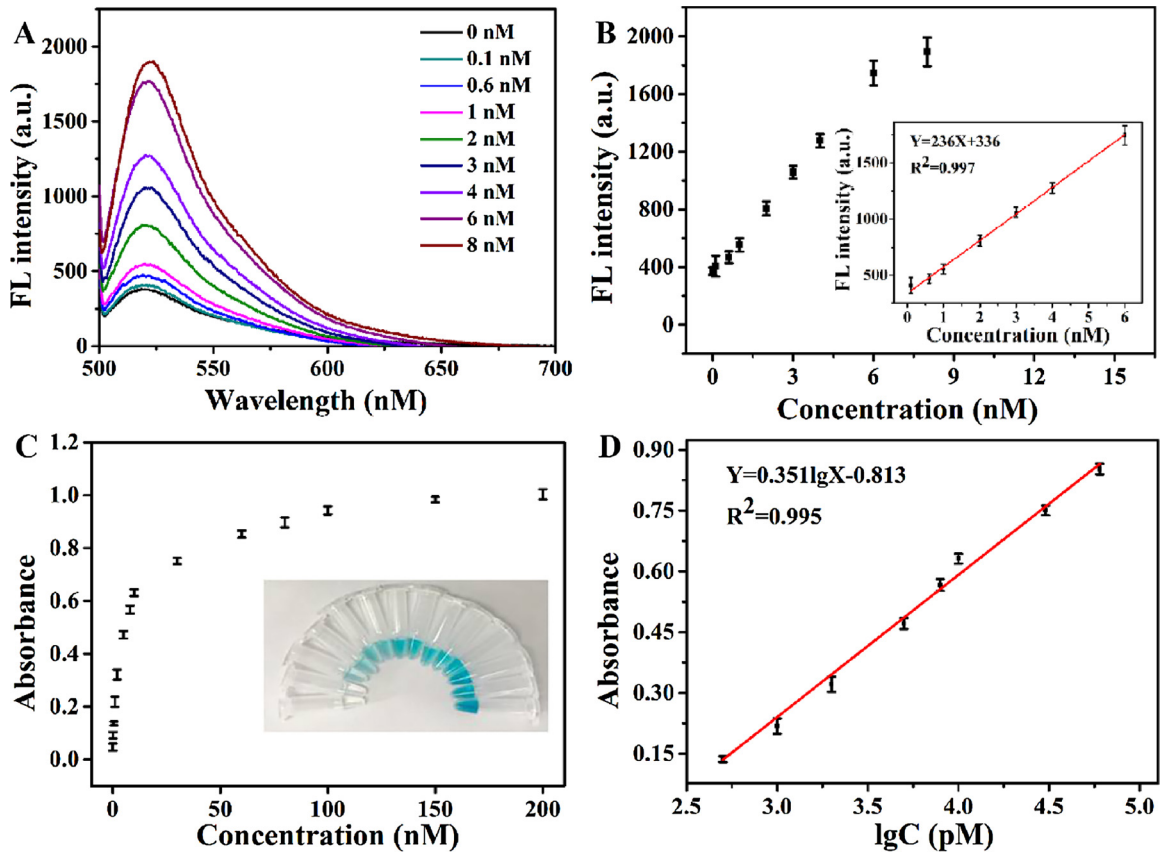

Fig. 5. Performance of dual-modal fluorescence and colorimetric measurements. (A) Fluorescent spectra of the detection system with different target concentrations (from bottom to top: 0 nM, 0.1 nM, 0.6 nM, 1 nM, 2 nM, 3 nM, 4 nM, 6 nM, 8 nM). (B) Linear relationship between fluorescent signal and target concentration. The inset shows the linear response from 0.1 nM to 6 nM. (C) Absorbance values of oxTMB at 452 nm plotted against different target concentrations. Inset shows naked-eye discernible color of corresponding samples. (D) Linear relationship between colorimetric signal and target concentration with the range from 500 pM to 60 nM.

3.3. Optimization of detection conditions

In order to confirm the optimal conditions for the detection of target, the incubation temperature for fluorescent assays, buffer composition, pH, and concentration of TMB and glucose for the colorimetric assays were systematically investigated. First, temperature was optimized ranging from 4 to 50 °C. As shown in Fig. 4A, the highest signal-to-background ratio (SBR) was observed at 37 °C. This was because the hairpin probes were too stable to be opened sequentially at lower temperature giving weak fluorescent signal, while they were not stable enough at higher temperature. Ultimately, 37 °C was used as the optimal temperature in further experiments. Next, given that the composition of the reaction buffer can affect colorimetric detection performance, the as-prepared DNA nanostructures were incubated in 4 different buffers: TBS buffer (0.025 M Tris, 0.14 M NaCl, 1 mM $MgCl_2$), HEPES buffer (10 mM HEPES, 140 mM NaCl), PBS buffer 1 (0.1 M NaCl, 0.1 M Na_2HPO_4, 0.1 M NaH_2PO_4), and PBS buffer 2 (0.1 M Na_2HPO_4, 0.1 M NaH_2PO_4). As shown in Fig. 4B, the maximum signal response was obtained in TBS buffer. Therefore, TBS was adopted as the optimum buffer. Moreover, pH 8.5 for colorimetric assay displayed the best performance (Fig. S3). The concentration effects of glucose and TMB were also evaluated in the colorimetric detection system. Since the rate-limiting step of the enzyme cascade reaction is the bioanalyzed oxidation of glucose, this controls the formation of oxTMB. The kinetics of the cascade followed a characteristic Michaelis-Menten kinetic model guided by the rate-limiting transformation [39]. As depicted in Fig. 4C, the initial velocity of the reaction increased gradually with increasing glucose concentration and then reached a plateau at 0.1 M glucose, which was chosen as the optimal glucose concentration. Meanwhile, the initial reaction rate increased along with the addition of TMB in the range of 0 to 0.6 mM, while the reaction rate decreased when TMB concentration increased further (Fig. 4D). Altogether, the optimized detection conditions are as follows: incubation of samples at 37 °C for 1 h for the fluorescent assay, and substrate solution containing 0.1 M glucose and 0.6 mM TMB in TBS buffer at pH 8.5 for the colorimetric assay.

3.4. Dual-modal detection of target

Under optimal conditions, the proposed strategy was employed to achieve dual-mode detection of target DNA. For fluorescent detection (Fig. 5A and B), it was clear to see that the enhancement of fluorescence was proportional to the concentration of target within the linear range from 0.1 to 6 nM. The regression equation was $Y = 0.236X + 336$ ($R^2 = 0.997$) with a detection limit of 15 pM (S/N = 3). Meanwhile, for colorimetric detection (Fig. 5C and D), it was obvious that gradual increase of the target concentration led to the generation of a darker solution via visual observation, and the absorbance value increased accordingly. The calibration plot was $Y = 0.351lgX - 0.813$ ($R^2 = 0.995$), and the detection limit was calculated to be 60 pM (S/N = 3). This detection performance was equivalent to or even better than some reported nanoparticle-, CHA-, or HCR-based amplified strategies for nucleotide detection (Table S2).

3.5. Specificity and reproducibility of the proposed strategy

To evaluate the practicability of the proposed dual-mode method, we further assessed the specificity and reproducibility respectively (Fig. 6). Assays were conducted by selecting 1 nM target DNA, 5 nM mismatched DNA, 5 nM deleted DNA, 5 nM inserted DNA, 5 nM random

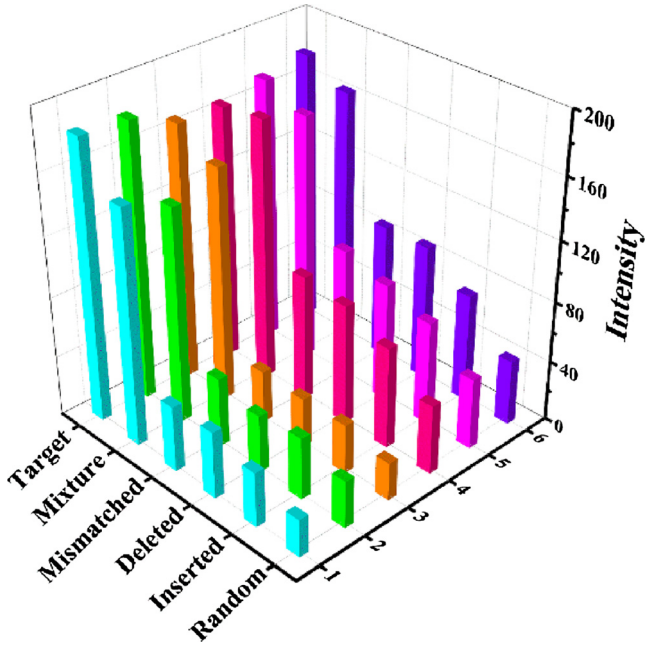

Fig. 6. Specificity and reproducibility of the dual mode measurement. Responses of fluorescence intensity (F-F_0, where F, F_0 are the fluorescence intensity of FAM in the presence or absence of corresponding DNA, respectively, (1) ~ (3)) and absorbance value (magnified 800×, (4) ~ (6)) changes of three hairpin probes with target DNA, random DNA, inserted DNA, deleted DNA, mismatched DNA and the mixture. The concentration used for target DNA was 1 nM and the others were 5 nM.

Table 1
Standard Addition Recovery Experiments of Target.

	Sample	Added (nM)	Detected (nM)	Recovery (%)	RSD (%, n = 3)
Fluorescent assay	1	0.5	0.47	94.0	1.8
	2	1	0.93	93.0	2.9
	3	5	5.33	106	3.3
Colormetric assay	1	0.5	0.46	92.0	5.6
	2	1	0.95	95.0	3.1
	3	5	5.49	109	3.9
	4	60	55.6	92.7	8.7

DNA, mixture including 1 nM target DNA, 5 nM mismatched DNA, 5 nM deleted DNA, 5 nM inserted DNA, and 5 nM random DNA. As demonstrated in Fig. 6, only target DNA and mixture caused a strong signal response, while minor changes were observed in the presence of any other DNA at a concentration of 5-fold than that of target, revealing satisfactory specificity of our proposed strategy. The reproducibility was also evaluated under the same conditions. As shown in Fig. 6 ((1) ~ (3) represent fluorescent assays, (4) ~ (6) represent colorimetric assays), six groups of target DNA detection were performed. The relative standard deviation (RSD) of fluorescent and colorimetric assays was 4.1% and 3.2%, respectively, indicating acceptable reproducibility for the proposed strategy.

3.6. Real sample analysis of target

FBS is typically the most widely used sample matrix to evaluate the applicability of the proposed strategy in complex samples, as demonstrated in the literature [1,40]. Therefore, in this study, FBS was selected as the complex fluid. Different concentrations of target RABV were added into the diluted FBS, and the recoveries of target were then recorded with the proposed strategy. The results are presented in Table 1. Satisfactory recoveries and acceptable standard deviations were achieved, thereby validating the reliability and practicality of the proposed strategy. Furthermore, three different concentrations of target were added into diluted healthy cerebrospinal fluid. The healthy cerebrospinal fluid was extracted from spinal cord of Sprague Dawley (SD) rats using a syringe [41]. The results in Table S3 indicate that the recoveries at different target content ranged from 96.0% to 106% with RSD values varying from 3.2% to 5.4%, and from 91.0% to 102% with RSD values varying from 3.3% to 7.1% for fluorescent and colorimetric assays, respectively, suggesting reliability of the strategy for applications in diluted cerebrospinal fluid.

4. Conclusion

In summary, an innovative fluorescent and colorimetric dual-mode strategy based on CHA was proposed for the detection of rabies virus oligonucleotide. As each target can trigger many reaction cycles forming Y-shaped DNA nanostructures, signal amplification is achieved, yielding a detection limit down to 15 pM and 60 pM for fluorescent and colorimetric readout, respectively. Moreover, the RSD of the fluorescent and colorimetric assays was 4.1% and 3.2%, respectively. The proposed strategy also showed excellent performance for target detection from biological media. Furthermore, a dual-mode sensor provides a chance for self-correction as opposed to single mode for quantitative detection of a series of nucleic acid-related biomarkers and even biological molecules with proper aptamers.

Declaration of Competing Interest

The authors declare no competing financial interest.

Acknowledgments

We gratefully appreciate the support from National Natural Science Foundation of China (21778020, 21804046, 21807036, 31750110464) and Sci-tech Innovation Foundation of Huazhong Agriculture University (2662017PY042).

Appendix A. Supplementary data

Supplementary material related to this article can be found, in the online version, at doi:https://doi.org/10.1016/j.snb.2019.127267.

References

[1] J. Zheng, X. Ji, M. Du, S. Tian, Z. He, Rational construction of a DNA nanomachine for HIV nucleic acid ultrasensitive sensing, Nanoscale 10 (2018) 17206–17211, https://doi.org/10.1039/C8NR05206A.
[2] L. Zou, L. Ling, Ultrasensitive detection of HIV DNA with polymerase chain reaction-dynamic light scattering, Anal. Chem. 90 (2018) 13373–13377, https://doi.org/10.1021/acs.analchem.8b03052.
[3] N. Yan, X. Wang, L. Lin, T. Song, P. Sun, H. Tian, et al., Gold nanorods electrostatically binding nucleic acid probe for in vivo microRNA amplified detection and photoacoustic imaging-guided photothermal therapy, Adv. Funct. Mater. 28 (2018) 1800490, , https://doi.org/10.1002/adfm.201800490.
[4] L. Zhang, S.R. Jean, X. Li, T. Sack, Z. Wang, S. Ahmed, et al., Programmable metal/semiconductor nanostructures for mRNA-modulated molecular delivery, Nano Lett. 18 (2018) 6222–6228, https://doi.org/10.1021/acs.nanolett.8b02263.
[5] W. Ma, P. Fu, M. Sun, L. Xu, H. Kuang, C. Xu, Dual quantification of microRNAs and telomerase in living cells, J. Am. Chem. Soc. 139 (2017) 11752–11759, https://doi.org/10.1021/jacs.7b03617.
[6] L. He, D. Lu, H. Liang, S. Xie, X. Zhang, Q. Liu, et al., mRNA-initiated, three-dimensional DNA amplifier able to function inside living cells, J. Am. Chem. Soc. 140 (2018) 258–263, https://doi.org/10.1021/jacs.7b09789.
[7] Y. Zhao, F. Chen, Q. Li, L. Wang, C. Fan, Isothermal amplification of nucleic acids, Chem. Rev. 115 (2015) 12491–12545, https://doi.org/10.1021/acs.chemrev.5b00428.
[8] H. Bui, S. Shah, R. Mokhtar, T. Song, S. Garg, J. Reif, Localized DNA hybridization chain reactions on DNA origami, ACS Nano 12 (2018) 1146–1155, https://doi.org/10.1021/acsnano.7b06699.
[9] L. Wu, G. Li, X. Xu, L. Zhu, R. Huang, X. Chen, Application of nano-ELISA in food analysis: recent advances and challenges, TrAC Trends Anal. Chem. 113 (2019) 140–156, https://doi.org/10.1016/j.trac.2019.02.002.

[10] H. Zhou, J. Liu, J.J. Xu, S.S. Zhang, H.Y. Chen, Optical nano-biosensing interface via nucleic acid amplification strategy: construction and application, Chem. Soc. Rev. 47 (2018) 1996–2019, https://doi.org/10.1039/C7CS00573C.
[11] W. Li, X. Yang, L. He, K. Wang, Q. Wang, J. Huang, et al., Self-assembled DNA nanocentipede as multivalent drug carrier for targeted delivery, ACS Appl. Mater. Interfaces 8 (2016) 25733–25740, https://doi.org/10.1039/C7CC01128H.
[12] S. Wang, S. Lu, J. Zhao, J. Ye, J. Huang, X. Yang, An electric potential modulated cascade of catalyzed hairpin assembly and rolling chain amplification for microRNA detection, Biosens. Bioelectron. 126 (2019) 565–571, https://doi.org/10.1039/c5ra26524j.
[13] Z. Gao, H. Xia, J. Zauberman, M. Tomaiuolo, J. Ping, Q. Zhang, et al., Detection of sub-fM DNA with target recycling and self-assembly amplification on graphene field-effect biosensors, Nano Lett. 18 (2018) 3509–3515, https://doi.org/10.1021/acs.nanolett.8b00572.
[14] Z. Wu, H. Fan, N.S.R. Satyavolu, W. Wang, R. Lake, J.H. Jiang, et al., Imaging endogenous metal ions in living cells using a DNAzyme-catalytic hairpin assembly probe, Angew. Chem. Int. Ed. 56 (2017) 8721–8725, https://doi.org/10.1002/anie.201703540.
[15] F. Li, H. Zhang, Z. Wang, X. Li, X.F. Li, X.C. Le, Dynamic DNA assemblies mediated by binding-induced DNA strand displacement, J. Am. Chem. Soc. 135 (2013) 2443–2446, https://doi.org/10.1021/ja311990w.
[16] J. Chen, S. Zhou, J. Wen, Concatenated logic circuits based on a three-way DNA junction: a keypad-lock security system with visible readout and an automatic reset function, Angew. Chem. Int. Ed. 54 (2015) 456–460, https://doi.org/10.1002/anie.201408334.
[17] S. Bi, S. Yue, S. Zhang, Hybridization chain reaction: a versatile molecular tool for biosensing, bioimaging, and biomedicine, Chem. Soc. Rev. 46 (2017) 4281–4298, https://doi.org/10.1039/C7CS00055C.
[18] F.C. Simmel, B. Yurke, H.R. Singh, Principles and applications of nucleic acid strand displacement reactions, Chem. Rev. 119 (2019) 6326–6369, https://doi.org/10.1021/acs.chemrev.8b00580.
[19] C. Liu, C. Chen, S. Li, H. Dong, W. Dai, T. Xu, et al., Target-triggered catalytic hairpin assembly-induced core-satellite nanostructures for high-sensitive "Off-to-On" SERS detection of intracellular MicroRNA, Anal. Chem. 90 (2018) 10591–10599, https://doi.org/10.1021/acs.analchem.8b02819.
[20] C. Wu, S. Cansiz, L. Zhang, I.T. Teng, L. Qiu, J. Li, et al., A nonenzymatic hairpin DNA cascade reaction provides high signal gain of mRNA imaging inside live cells, J. Am. Chem. Soc. 137 (2015) 4900–4903, https://doi.org/10.1021/jacs.5b00542.
[21] F.X. Su, C.X. Yang, X.P. Yan, Intracellular Messenger RNA triggered catalytic hairpin assembly for fluorescence imaging guided photothermal therapy, Anal. Chem. 89 (2017) 7277–7281, https://doi.org/10.1021/acs.analchem.7b01348.
[22] J. Dai, H. He, Z. Duan, Y. Guo, D. Xiao, Self-replicating catalyzed hairpin assembly for rapid signal amplification, Anal. Chem. 89 (2017) 11971–11975, https://doi.org/10.1021/acs.analchem.7b01946.
[23] P. Yin, H.M. Choi, C.R. Calvert, N.A. Pierce, Programming biomolecular self-assembly pathways, Nature 451 (2008) 318–322, https://doi.org/10.1038/nature06451.
[24] Y. Li, Y. Chang, R. Yuan, Y. Chai, Highly efficient target recycling-based netlike Y-DNA for regulation of electrocatalysis toward methylene blue for sensitive DNA detection, ACS Appl. Mater. Interfaces 10 (2018) 25213–25218, https://doi.org/10.1021/acsami.8b08545.
[25] C. Xue, S.X. Zhang, C.H. Ouyang, D. Chang, B.J. Salena, Y. Li, et al., Target-induced catalytic assembly of Y-shaped DNA and its application for in situ imaging of MicroRNAs, Angew. Chem. Int. Ed. 57 (2018) 9739–9743, https://doi.org/10.1002/anie.201804741.
[26] Z. Qing, X. He, J. Huang, K. Wang, Z. Zou, T. Qing, et al., Target-catalyzed dynamic assembly-based pyrene excimer switching for enzyme-free nucleic acid amplified detection, Anal. Chem. 86 (2014) 4934–4939, https://doi.org/10.1021/ac500834g.
[27] S. Lu, T. Hu, S. Wang, J. Sun, X. Yang, Ultra-sensitive colorimetric assay system based on the hybridization chain reaction-triggered enzyme cascade amplification, ACS Appl. Mater. Interfaces 9 (2017) 167–175, https://doi.org/10.1021/acsami.6b13201.
[28] M. Liu, J. Fu, C. Hejesen, Y. Yang, N.W. Woodbury, K. Gothelf, et al., A DNA tweezer-actuated enzyme nanoreactor, Nat. Commun. 4 (2013) 2127, https://doi.org/10.1038/ncomms3127.
[29] L. Xin, C. Zhou, Z. Yang, D. Liu, Regulation of an enzyme cascade reaction by a DNA machine, Small 9 (2013) 3088–3091, https://doi.org/10.1039/C8TB02659A.
[30] L. Sun, Y. Gao, Y. Xu, J. Chao, H. Liu, L. Wang, et al., Real-time imaging of single-molecule enzyme cascade using a DNA origami raft, J. Am. Chem. Soc. 139 (2017) 17525–17532, https://doi.org/10.1021/jacs.7b09323.
[31] Y. Chen, G. Ke, Y. Ma, Z. Zhu, M. Liu, Y. Liu, et al., A synthetic light-driven substrate channeling system for precise regulation of enzyme cascade activity based on DNA origami, J. Am. Chem. Soc. 140 (2018) 8990–8996, https://doi.org/10.1021/jacs.8b05429.
[32] X. Wei, T. Tian, S. Jia, Z. Zhu, Y. Ma, J. Sun, et al., Microfluidic distance readout sweet hydrogel integrated paper-based analytical device (muDiSH-PAD) for visual quantitative point-of-care testing, Anal. Chem. 88 (2016) 2345–2352, https://doi.org/10.1021/acs.analchem.5b04294.
[33] M. Faye, L. Dacheux, M. Weidmann, S.A. Diop, C. Loucoubar, H. Bourhy, et al., Development and validation of sensitive real-time RT-PCR assay for broad detection of rabies virus, J. Virol. Methods 243 (2017) 120–130, https://doi.org/10.1016/j.jviromet.2016.12.019.
[34] C.R. Fisher, D.G. Streicker, M.J. Schnell, The spread and evolution of rabies virus: conquering new frontiers, Nat. Rev. Microbiol. 16 (2018) 241–255, https://doi.org/10.1038/nrmicro.2018.11.
[35] A. Deubelbeiss, M.-L. Zahno, M. Zanoni, D. Bruegger, R. Zanoni, Real-time RT-PCR for the detection of lyssavirus species, J. Vet. Med. 2014 (2014) 1–12, https://doi.org/10.1155/2014/476091.
[36] S.A. Nadin-Davis, M. Sheen, A.I. Wandeler, Development of real-time reverse transcriptase polymerase chain reaction methods for human rabies diagnosis, J. Med. Virol. 81 (2009) 1484–1497, https://doi.org/10.1002/jmv.21547.
[37] O.I. Wilner, Y. Weizmann, R. Gill, O. Lioubashevski, R. Freeman, I. Willner, Enzyme cascades activated on topologically programmed DNA scaffolds, Nat. Nanotechnol. 4 (2009) 249–254, https://doi.org/10.1038/nnano.2009.50.
[38] J. Fu, M. Liu, Y. Liu, N.W. Woodbury, H. Yan, Interenzyme substrate diffusion for an enzyme cascade organized on spatially addressable DNA nanostructures, J. Am. Chem. Soc. 134 (2012) 5516–5519, https://doi.org/10.1021/ja300897h.
[39] L. Wu, W. Yin, K. Tang, K. Shao, Q. Li, P. Wang, et al., Highly sensitive enzyme-free immunosorbent assay for porcine circovirus type 2 antibody using Au-Pt/SiO2 nanocomposites as labels, Biosens. Bioelectron. 82 (2016) 177–184, https://doi.org/10.1016/j.bios.2016.04.001.
[40] T. Wu, Y. Cao, Y. Yang, X. Zhang, S. Wang, L. Xu, et al., A three-dimensional DNA walking machine for the ultrasensitive dual-modal detection of miRNA using a fluorometer and personal glucose meter, Nanoscale 11 (2019) 11279–11284, https://doi.org/10.1039/C9NR03588E.
[41] Y.L. Lai, P.M. Smith, W.J. Lamm, J. Hildebrandt, Sampling and analysis of cerebrospinal fluid for chronic studies in awake rats, J. Appl. Physiol. 54 (1983) 1754–1757, https://doi.org/10.1152/jappl.1983.54.6.1754.

Jiaojiao Zhou is a PhD student from college of food science and technology.

Wenjing Wang is an associate research fellow at Huazhong Agricultural University. Dr. Wang received her PhD degree in 2017 from school of chemistry and chemical engineering, Nanjing University. Her research mainly focuses on biochemical analysis, DNA nano-technology, molecular imaging.

Shuojun Li is a graduate student major in chemistry.

Axiu Nie is a graduate student major in chemistry.

Zhiyong Song received his PhD degree in Department of Chemistry from Zhejiang University in 2015. His current research interests include the chemical and biological effects of nanomaterials on bacteria and viruses.

Mohamed F. Foda received his PhD degree in 2015 from college of life science and technology, Huazhong Agricultural University. Now he works as a postdoctoral fellow at Huazhong Agricultural University. His scientific interests involve biosensors, nanomaterial systhesis and virus research.

Zhicheng Lu received his Ph.D. in 2008 from Jilin University. His research mainly focuses on SERS and its applications in chemical sensing and biosensing.

Ling Zhao earned his M.S. and his Ph.D. from Huazhong Agricultural University in 2005 and University of Georgia in 2009, respectively. He joined the Department of Microbiology and Immunology at University of Pennsylvania School of Medicine and completed his postdoctoral research from 2009 to 2012. He has been appointed as a Professor at College of Veterinary Medicine, Huazhong Agricultural University since 2012. His current research are focused on immunobiology and pathogenesis of rabies virus.

Heyou Han is a professor in the State Key Laboratory of Agricultural Microbiology, College of Science from Huazhong Agricultural University (China). He received his PhD in analytic chemistry from the Wuhan University in 2000. From 2000 to 2002, he was a post-doctoral researcher at the University of Science and Technology of China. His research area mainly focuses on developing new analysis methods to detect pathogenic microorganisms including virus and bacteria in agriculture. He is also interested in tumor bioimaging and therapy.